

Article

# Selective Furfuryl Alcohol Production from Furfural via Bio-Electrocatalysis

Peng Zhan <sup>1,†</sup>, Xiangshi Liu <sup>2,†</sup>, Qian Zhu <sup>1</sup>, Hongqing Zhao <sup>1</sup>, Shiding Zhang <sup>1</sup>, Chenxi Zhang <sup>1</sup>, Cong Ren <sup>1</sup>, Jiawen Zhang <sup>1</sup>, Changwei Zhang <sup>1</sup> and Di Cai <sup>1,\*</sup>

<sup>1</sup> National Energy R&D Center for Biorefinery, Beijing University of Chemical Technology, Beijing 100029, China

<sup>2</sup> College of Life Science and Technology, Beijing University of Chemical Technology, Beijing 100029, China

\* Correspondence: caidibuct@163.com

† These authors contributed equally to this work.

**Abstract:** The catalytic reduction of renewable furfural into furfuryl alcohol for various applications is in the ascendant. Nonetheless, the conventional chemo-catalysis hydrogenation of furfural always suffers from poor selectivity, harsh conditions, and expensive catalysts. Herein, to overcome the serious technical barriers of conventional furfuryl alcohol production, an alternative bio-electrocatalytic hydrogenation system was established under mild and neutral conditions, where the dissolved cofactor (NADH) and the alcohol dehydrogenase (ADH) participated in a tandem reaction driven by the electron from a novel Rh (III) complex fixed cathode. Under the optimized conditions, 81.5% of furfural alcohol selectivity can be realized at  $-0.43$  V vs. RHE. This contribution presents a ‘green’ and promising route for the valorization of furfural and other biomass compounds.

**Keywords:** bio-electrocatalysis; furfuryl alcohol; furfural reduction; Rh (III) complex; alcohol dehydrogenase



**Citation:** Zhan, P.; Liu, X.; Zhu, Q.; Zhao, H.; Zhang, S.; Zhang, C.; Ren, C.; Zhang, J.; Zhang, C.; Cai, D. Selective Furfuryl Alcohol Production from Furfural via Bio-Electrocatalysis. *Catalysts* **2023**, *13*, 101. <https://doi.org/10.3390/catal13010101>

Academic Editor: Binlin Dou

Received: 28 November 2022

Revised: 19 December 2022

Accepted: 27 December 2022

Published: 3 January 2023



**Copyright:** © 2023 by the authors. Licensee MDPI, Basel, Switzerland. This article is an open access article distributed under the terms and conditions of the Creative Commons Attribution (CC BY) license (<https://creativecommons.org/licenses/by/4.0/>).

## 1. Introduction

The production of renewable biochemicals from the abundant lignocellulosic biomass is considered a practical alternative to address the issues of tremendous consumption of fossil energy resources and global climate change [1,2]. Furfural, derived from the hemicelluloses in lignocelluloses matrix, is regarded as a primary platform chemical for a variety of valuable fuels and chemicals [3]. For instance, furfuryl alcohol, obtained from furfural after selective hydrogenation, is regarded as a promising molecule that has been extensively applied in the food, pharmaceutical, and polymers industries [4–6].

As for the potential routes for catalytic furfuryl alcohol production from furfural, in contrast to the traditional thermo-chemical hydrogenation by expensive noble metal catalysts and organic solvents under severe conditions [7–10], recently, the biocatalytic furfuryl alcohol production by enzymes or whole-cells has attracted much attention owing to the superiorities of the mild conditions, extraordinary selectivity, the low-cost, and low-pollutions [11,12]. In a typical biological process for furfural hydrogenation, an *ex vivo* or *in vivo* alcohol dehydrogenase (ADH) is commonly used [13], where a cofactor, normally the nicotinamide adenine dinucleotide (NADH), acts as the reduction force to actuate the reaction [14]. The mechanism for bio-catalysis transformation of furfural into furfuryl alcohol by ADH is clear. Generally, NADH gives hydrogen and an electron, and subsequently transforms into  $\text{NAD}^+$  [15], while stoichiometrically, one mole of furfuryl alcohol can be generated from one mole of furfural using the hydrogen atom and electron from NADH [16,17]. In this process, the rate-limiting step of the furfural biohydrogenation is the speed of NADH regeneration [18].

To realize effective NADH regeneration in typical whole-cell catalysis process, sugars are required in the initial substrate and are served as the energy source to guarantee the supplementation of the reduction force in living cells. However, the sugar metabolism induces the side reactions, and the by-products further cause complex downstream furfuryl

alcohol separations. Another weakness of the whole-cell catalysis process is the poor tolerance of furfural in living cells [19,20]. Consequently, the low furfural concentration in substrate limits the bio-catalysis efficiency. In the enzymatic hydrogenation process, the effective regeneration of the ex vivo NADH is recognized as a decisive factor in the high furfuryl alcohol production efficiency [21]. Among the commonly used ex vivo NADH regeneration methods, including the biological, chemical, photo-chemical, and electro-chemical routes, the electro-chemical regeneration of NADH exhibited obvious advantages of trace number of by-products, convenient product recovering, and the potential usage of renewable electricity [22–24], and the corresponding bio-electrochemical system has been applied in various chemical production processes [25–27].

In the electro-enzymatic catalysis process, the effective electron transfer between the electrode and the  $\text{NAD}^+$  should be concerned so as to realize a high NADH regeneration rate [28]. The redox mediator Rh-complex ( $\text{M} = [\text{Cp}^*\text{Rh(III)(bpy)Cl}]^+$ ,  $\text{Cp}^*$  = pentamethylcyclopentadienyl,  $\text{bpy} = 2,2'$ -bipyridine) is suggested as an efficient electronic mediator for the  $\text{NAD}^+$  reduction to NADH [29,30], which exhibits outstanding performance in facilitating the NADH regeneration and restraining the undesired by-products (e.g.,  $\text{NAD}_2$  dimer) [31]. In previous research, the suspended Rh-complex was involved in photo-catalytic NADH regeneration. After hybridizing the ADH with the semiconductor photocatalyst for furfural biohydrogenation, a high furfuryl alcohol selectivity (nearly 100%) can be realized [32]. However, the primary limitation of the process is the difficulties in Rh-complex recovery from the homogeneous reactant [33]. In order to overcome the obstacle, the immobilization of Rh-complex on the surface of electrodes is proved as an efficient way [34]. For instance, high faradic efficiency of 97% for NADH regeneration can be realized on an electrode made of Rh-modified NU-1000 films [35].

Herein, for the first time, bio-electrocatalytic hydrogenation of furfural into more valuable furfuryl alcohol was realized by integrating the ex vivo NADH regeneration with enzyme reaction in an H-cell. To actualize high NADH regeneration in the bio-electrocatalysis process, Rh-complex, the redox mediator, was fixed on the surface of amino-modified carbon paper and served as the cathode. After the characterization of the novel Rh-complex fixed cathode and investigation of the NADH regeneration performances, the bio-electrocatalysis system for furfuryl alcohol production from furfural was conducted by introducing ADH and  $\text{NAD}^+$  into the buffer. Results indicated the novel bio-electrocatalytic process exhibited high furfuryl alcohol yield and selectivity. The bio-electrocatalysis system also showed a lot of promises in other biochemical valorizations.

## 2. Results and Discussion

### 2.1. Characterization of the Rh-Complex Fixed Electrode

The Rh-complex fixed electrode to be used in bio-electrocatalytic hydrogenation of furfural into furfuryl alcohol was prepared and characterized. SEM morphology suggested the Rh-complex presents an irregular block structure (Figure 1a). Meanwhile, the cross-section SEM image of the Rh-complex fixed electrode (Figure 1b) proves the Rh-complex was evenly loaded on the surface of amino-modified carbon paper. Elemental mappings of the Rh-complex fixed electrode (Figure 1c and Figure S2) further illustrated the uniform distribution of Rh element and N element on the surface of the functionalized electrode, demonstrating the successful introduction of amino groups and the conjugation of the Rh-complex onto the amino-modified carbon paper.

X-ray photoelectron spectroscopy (XPS) measurements were further adopted to identify the chemical composition and valence states of the Rh-complex. As shown in Figure 1d, the characteristic peak of Rh was detected, confirming the successful construction of the Rh-complex on the surface of the amino-modified carbon paper. The XPS spectrum also indicated that Rh  $3d_{5/2}$  and Rh  $3d_{3/2}$  are composed of the Rh (III) complex (309.8 and 314.2 eV, respectively) [36]. The O  $1s$  and C  $1s$  spectrum indicated the carboxyl group was effectively introduced into the Rh-complex (Figure S3). Besides, the PXRD patterns suggested that the Rh-complex maintained a certain crystallinity rather than amorphousness (Figure S4). Fur-

thermore,  $^1\text{H}$  NMR (MeOD as solvent) was conducted to analyze the chemical structure of the synthesized Rh-complex (Figure 1e). The characteristic signals at 9.49 and 8.79 ppm can be assigned to the chemical structure of 2,2'-bipyridine-5,5'-dicarboxylic acid, suggesting the effective chelation of the Rh precursor.

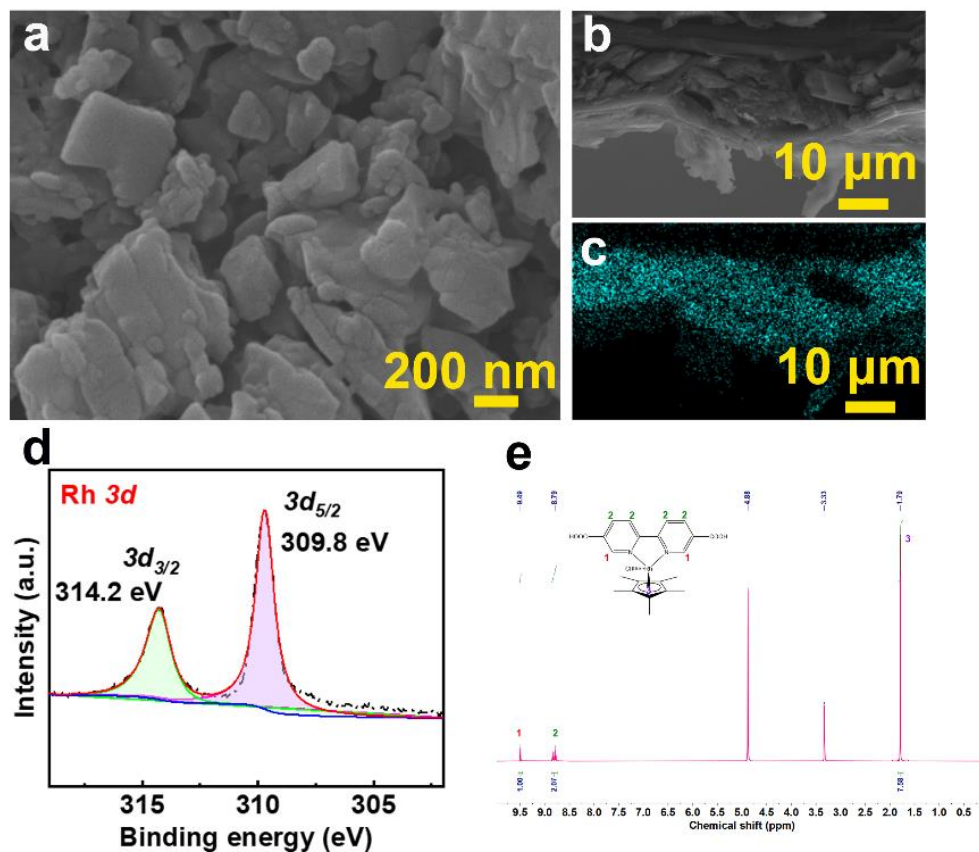


**Figure 1.** Characterizations of the Rh-complex. (a) SEM image of the Rh-complex, (b) cross section SEM image and (c) elemental mappings of the Rh-complex fixed electrode. (d) The Rh 3d XPS spectrum, and (e)  $^1\text{H}$  NMR spectrum of the Rh-complex.

## 2.2. Catalytic Regeneration of NADH by the Rh-Complex Fixed Electrode

The priority in bio-electrocatalytic hydrogenation of furfural is efficient NADH regeneration with high sustainability and stability [37]. Therefore, in this section, the performance of electrocatalytic reduction of  $\text{NAD}^+$  into NADH was investigated using the Rh-complex fixed electrode in an H-cell. The CV curves of the Rh-complex fixed electrode were analyzed to investigate the electrocatalytic activity of  $\text{NAD}^+$  reduction. The CVs of the Rh-complex were collected with the potential range from 0.7 to  $-0.8$  V (vs. RHE). As shown in Figure 2a, a reduction peak at  $-0.22$  V vs. RHE and an oxidation peak at  $-0.08$  V vs. RHE appeared, inferring the Rh (III) was reduced to the Rh (I) on the surface of the cathode and the adsorption and desorption of protons occurred on the Rh-complex [28,38]. Besides, the reductive current peak of the Rh-complex after the addition of the  $\text{NAD}^+$  ( $2.9 \text{ mA cm}^{-2}$ ) was significantly higher than the  $\text{NAD}^+$  absent system ( $1.6 \text{ mA cm}^{-2}$ ), reflecting the reduction of the  $\text{NAD}^+$  [35]. Moreover, no reduction peak or oxidation peak was observed in the CV curves, and the current density was always maintained at a low level on the bare amino-modified electrode. All the aforementioned phenomena suggest the NADH regeneration on the Rh-complex fixed electrode can be realized by a two-step process. In the first step, the Rh (III) was reduced to the Rh (I), which was driven by the applied potentials. Subsequently, in the second step, the shuttling  $\text{NAD}^+$  on the surface of the electrical double layer quickly combined with the Rh (I), and regenerated the NADH [39].

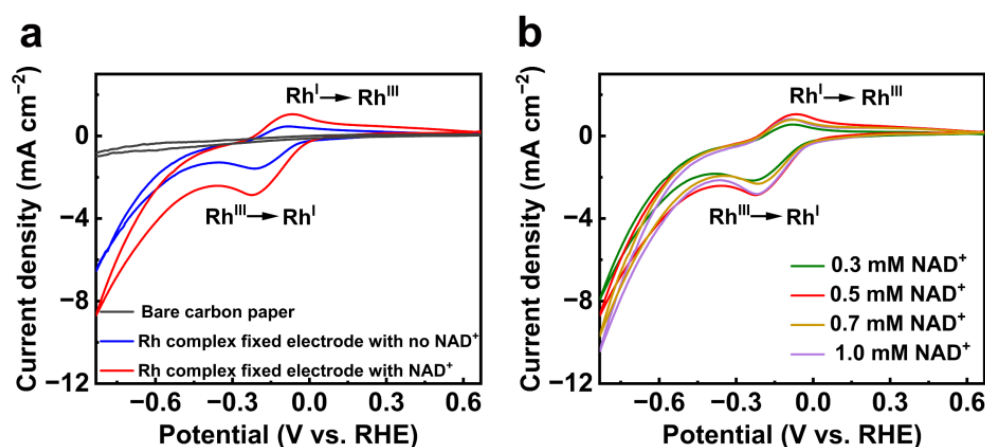


**Figure 2.** (a) CV curves of the bare carbon paper electrode and the Rh-complex fixed electrode with or without NAD<sup>+</sup> in PBS buffer; (b) CV curves of Rh-complex with different concentrations of NAD<sup>+</sup>. The scan rate was 20 mV s<sup>-1</sup>.

In order to better understand the NADH regeneration mechanism in the electrocatalysis process, CV curves of the Rh-complex fixed electrode with different NAD<sup>+</sup> dosages in buffer were further investigated. Figure 2b clearly shows that the reductive current peak at -0.22 V vs. RHE raised rapidly with the increase of NAD<sup>+</sup> concentration in buffer, implying the Rh-complex fixed electrode possessed a significant electrocatalytic performance in NAD<sup>+</sup> reduction [38].

The NADH regeneration efficiency by the Rh-complex fixed electrode was analyzed using 0.5 mM of NAD<sup>+</sup> solution. As presented in Figure 3, the equilibrium of NAD<sup>+</sup> reduction appeared within 30 min of reaction at -0.43 V vs. RHE, and the conversion of NAD<sup>+</sup> reached 87.4%. As expected, in the control group using a similar cathode without the applied potential, the NADH was barely detected in the buffer at the end of the reaction, suggesting that certain applied potential is the precondition for the NADH regeneration in the electrocatalytic process. These results are as comparative as the results in the literature using other types of cathodes. For instance, a high yield of NADH (80.75%) was reported using the Rh-complex-grafted electrode [39]. Chen et al. also introduced an Rh-FTO glass electrode to regenerate NADH with a conversion rate of more than 90% at -1.1 V vs. Ag/AgCl [40].

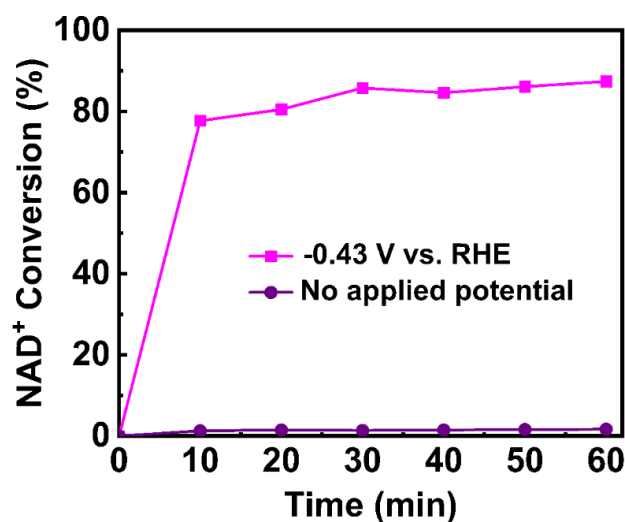


**Figure 3.** NAD<sup>+</sup> conversion by the Rh-complex fixed electrode with or without the applied potential.

### 2.3. Bio-Electrocatalysis Production of Furfuryl Alcohol from Furfural

The attractive NADH regeneration performances of the Rh (III) complex fixed electrode derived us to further extend the system to bio-electrocatalytic hydrogenation of furfural into furfuryl alcohol. In the bio-electrocatalysis process, the as-prepared Rh-complex fixed electrode was adopted to provide sustainable and stable NADH, whilst ADH was used for catalytic reduction of furfural that was driven by the regenerated NADH. The bio-electrocatalysis was carried out using 0.1 M phosphate buffer (PBS, 0.1 M, pH = 8) with 0.5 mM of NAD<sup>+</sup> and 0.5 mM of furfural, and the effect of applied potentials on furfuryl alcohol production was evaluated. As can be seen from Figure 4a, a volcano-like trend of furfuryl alcohol selectivity was obtained along the change of voltage. A maximum furfuryl alcohol selectivity of 81.5% with a conversion of 56.1% was obtained at  $-0.43$  V vs. RHE. Besides, relatively lower furfuryl alcohol selectivity appeared when the applied potentials were above  $-0.43$  V vs. RHE, which can be attributed to the increase of the competitive hydrogen evolution reaction (HER) [41]. The yields of furfuryl alcohol follow the same trend of the selectivity, reaching a maximum of 45.7% at  $-0.43$  V vs. RHE. The conversion of furfural, however, continuously increased with the increase of the applied potentials and finally reached 61.0% at  $-0.63$  V vs. RHE. As expected, the current densities for furfural hydrogenation over different applied potentials suggested the current densities raised along with the increase of the charged potentials (Figure S5).

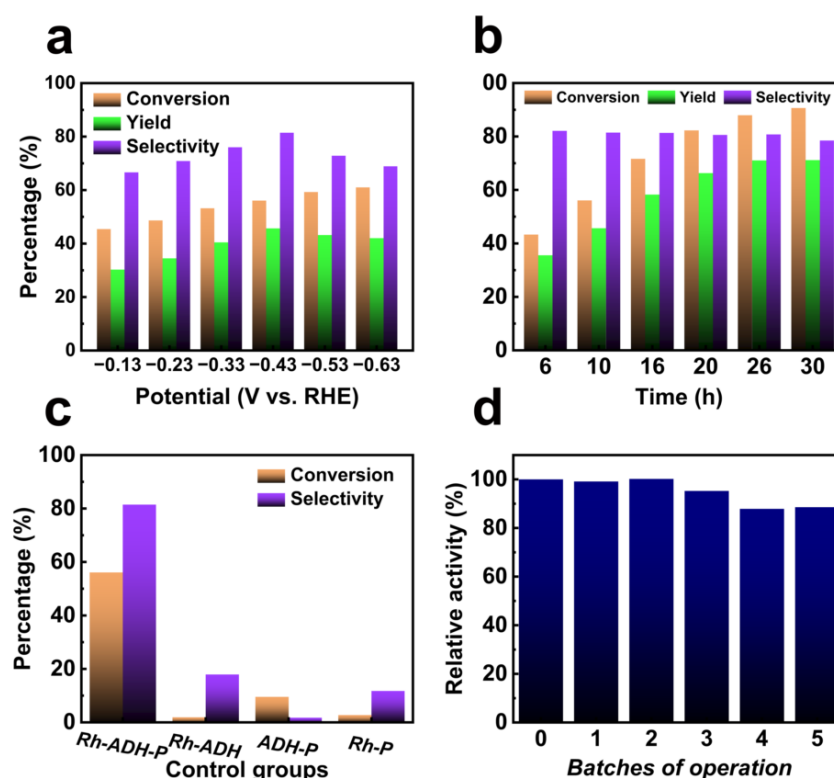


**Figure 4.** Bio-electrocatalytic reduction of furfural into furfuryl alcohol using the Rh-complex fixed electrode. (a) The effect of the applied potentials on furfuryl alcohol production, (b) time course of the bio-electrocatalysis furfural transformation at  $-0.43$  V vs. RHE, (c) comparison of the bio-electrocatalytic furfural conversion and the furfuryl alcohol yield with the control groups. Rh-ADH-P: The Rh-complex fixed electrode with ADH and the applied potential, Rh-ADH: The Rh-complex fixed electrode with ADH and no applied potential, ADH-P: Bare amino-modified carbon paper with ADH and the applied potential, Rh-P: The Rh-complex fixed electrode with the applied potential and without ADH, (d) stability of the bio-electrocatalytic reduction of furfural into furfuryl alcohol using the recovered Rh-complex fixed electrode.

The time course of the bio-electrocatalysis of furfural was investigated using the Rh-complex fixed electrode at  $-0.43$  V vs. RHE in order to better understand the catalytic kinetics of the furfural hydrogenation process. As it is shown in Figure 4a, the furfural conversion constantly increased with the prolongation of the reaction time, and finally reached 90.6% at 30 h. The furfuryl alcohol selectivity generally maintained around ~80% in the entire period of reaction. Due to the formation of by-products, it slightly decreased with the increase in reaction time.

To verify the synergistic effect of the Rh-complex fixed electrode and ADH on furfuryl alcohol production, several groups of control experiments were also conducted. As illuminated in Figure 4c, the furfuryl alcohol can be barely detected on the Rh-complex fixed electrode with ADH and no applied potential in  $\text{NAD}^+$  contained electrolyte, implying the regenerated of NADH requires electricity as the energy resource. Additionally, there was almost no furfuryl alcohol production when using bare amino-modified carbon paper with ADH, and the applied potential in  $\text{NAD}^+$  contained electrolyte, indicating only NADH can be utilized as the reduction force by ADH. Moreover, a trace amount of furfuryl alcohol was obtained in the group using the Rh-complex fixed electrode with the applied potential and absent with ADH, suggesting ADH is the main biological catalyst for furfural hydrogenation.

The stability of the bio-electrocatalysis system was further explored. For each batch of operation (30 h of reaction was performed for every cycle), the Rh-complex fixed electrode was washed, recycled, and reused for the following batches of bio-electrocatalysis. As shown in Figure 4d, after five batches of operation, the recovered electrode still sustained a remarkably high selectivity towards furfuryl alcohol, although the catalytic performance slightly went down with the increase of the recycling times owing to the exfoliation of Rh-complex on the electrode surface [11]. Specifically, the relative activity of the furfuryl alcohol (compared with the primordial furfuryl alcohol selectivity) remained up to 88.6% using the recycled Rh-complex fixed electrode after five cycles.

Therefore, the tandem electro-chemical regeneration of the NADH and enzymatic reaction for selective hydrogenation of the aldehyde group in furfural molecule paves the way to combine the advantages of both electrocatalysis and enzymic catalysis. In this case, the Rh-complex fixed on the amino-modified carbon paper provided a sustainable and stable method for NADH regeneration. Meanwhile, ADH distributed in the electrical double layer efficiently performed both the electroenzymatic furfural hydrogenation and simultaneous cofactor regeneration [40].

### 3. Materials and Methods

#### 3.1. Materials

Reduced and oxidized nicotinamide adenine dinucleotide ( $\text{NADH}/\text{NAD}^+$ , 98 wt%), and alcohol dehydrogenase (ADH, 1981.2 U/mg) from *Saccharomyces cerevisiae* were purchased from Shanghai Yuanye Bio-Technology Co., Ltd. Furfural, furfuryl alcohol, potassium phosphate dibasic, potassium phosphate dibasic trihydrate, poly(ethyleneimine) (PEI), dopamine hydrochloride (DA), ether, 2,2'-bipyridyl-5,5'-dicarboxylic acid, dichloro-(pentamethylcyclopentadienyl) rhodium (III) dimer ( $[\text{Cp}^*\text{RhCl}_2]_2$ ), and methanol were obtained from Shanghai Macklin Biochemical Co., Ltd. (Shanghai, China). Unless otherwise stated, the above chemicals were all under analytical grade and were used as received. Nafion N-117 membrane (0.180 mm thick), Toray carbon paper (CP, TGP-H-60, 20 cm  $\times$  20 cm), and Nafion D-521 dispersion were provided by Alfa Aesar China Co., Ltd. (Shanghai, China) Deionized water (18.2  $\text{M}\Omega$   $\text{cm}^{-1}$ ) was used in all experiments.

#### 3.2. Preparation of the Rh-Complex Fixed Electrode

The Rh-complex was synthesized according to the reported method [42]. Typically,  $[\text{Cp}^*\text{RhCl}_2]_2$  (61.8 mg) and 2,2'-bipyridine-5,5'-dicarboxylic acid (48.8 mg) were mixed in 15 mL of methanol, followed by stirring the mixture at 300 rpm for 6 h at room temperature ( $\sim 25$  °C). Subsequently, excess diethyl ether was added to the suspension. After centrifu-

gation at 10,000 rpm for 5 min, the solid fraction was collected, and the Rh-complex was obtained after vacuum drying at 40 °C.

As for the preparation of the Rh-complex fixed electrode, carbon paper was first modified with amino groups according to the literature [43]. Briefly, carbon paper (1 cm × 1 cm) was ultrasonic in deionized water, ethanol, and acetone for 15 min, respectively. Then, 2 mg mL<sup>-1</sup> of PDI and 2 mg mL<sup>-1</sup> of PEI were added into Tris-HCl buffer (pH = 8.5) under vigorous stirring at room temperature (~25 °C), and the ultrasonic pretreated carbon paper was coprecipitated with PDI and PEI solutions. After stirring at a speed of 400 rpm for 10 h, the received amino-groups functionalized carbon paper was cleaned by deionized water three times, and dried out in vacuum.

Then, the Rh-complex was loaded on the as-prepared amino-modified carbon paper, according to the protocol as follows: 2 mg of Rh-complex suspended in 200 µL of methanol was uniformly drop-casted on the surface of the as-prepared amino-modified carbon paper. Subsequently, 10% (v/v) Nafion solution (20 µL Nafion in 200 µL methanol) was loaded. After drying out at room temperature (~25 °C), the Rh-complex fixed electrode was gathered and stored at 4 °C before use. For more details on the electrode preparation process, please see Figure S1.

### 3.3. Electro-Chemical NADH Regeneration

A typical H-cell with two compartments separated by a cation exchange membrane (Nafion N-117) was conducted to analyze the electro-chemical NADH regeneration behaviors on a CHI760E workstation (Shanghai CH Instruments Co., Shanghai, China) at room temperature (~25 °C). The Rh-complex fixed electrode was used as the working electrode, while the Ag/AgCl (3.5 M KCl) electrode was equipped as the reference electrode. Besides, the platinum gauze served as the counter electrode. 0.1 M of phosphate buffer (PBS, pH = 8) was applied as the electrolytes in both anode and cathode chambers. Before the electro-chemical catalysis carried out, the electrolytes were purged with N<sub>2</sub> for 30 min to remove the dissolved oxygen. The cyclic voltammetry (CV) curves were measured in the NAD<sup>+</sup> solution with a scan rate of 20 mV s<sup>-1</sup> under the potential range from 0.7 to -0.8 V vs. RHE. Electrolysis was performed to accomplish the regeneration of NADH from NAD<sup>+</sup> using the Rh-complex fixed electrode at -0.43 V vs. Ag/AgCl.

### 3.4. Bio-Electrocatalytic Hydrogenation of Furfural

The bio-electrocatalytic hydrogenation of furfural into furfuryl alcohol was implemented in an H-cell (Figure S6) that was equipped with three electrodes. Generally, 2 mg of ADH was uniformly dispersed in 30 mL of PBS buffer (pH = 8) that containing 0.5 mM of NAD<sup>+</sup> and 0.5 mM of furfural in the cathode chamber. Then, the Rh-complex fixed electrode was immersed in the catholyte for 0.5 h before the reaction. Finally, the bio-electrocatalytic hydrogenation of furfural was performed at different applied potentials (-0.13 V to -0.63 V vs. Ag/AgCl).

### 3.5. Assay

Scanning electron microscope (SEM) images and Scanning Electron Microscope-Energy Dispersive X-Ray Spectroscopy (SEM-EDX) images were gathered from Zeiss Gemini 300. X-ray diffraction (XRD) patterns were performed on a Bruker D8 Advance X-ray diffractometer using Cu K $\alpha$  radiation ( $\lambda = 1.54184 \text{ \AA}$ ). X-ray photoelectron spectroscopy (XPS) was implemented by a SHIMADZU Kratos AXIS SUPRA spectrometer. <sup>1</sup>H nuclear magnetic resonance (<sup>1</sup>H NMR) was conducted to investigate the chemical structure of the as-prepared Rh-complex on Bruker AVANCE III HD 400.

The NADH concentration was detected by ultraviolet and visible spectrophotometer (Shanghai Spectrum Instruments Co., Ltd., Shanghai, China) at 340 nm, and the standard curve of NADH can be seen in Figure S7. The bio-electrocatalysis products were analyzed as follows: High-performance liquid chromatography (HPLC) that was equipped with an ultraviolet (UV) detector was adopted to detect the concentration of furfural and furfuryl

alcohol in the electrolytes. Next, 55% (v/v) acetonitrile and 45% (v/v) ultrapure water served as the mobile phase. The flow rate of the mobile phase was 0.5 mL min<sup>-1</sup>. The standard curves of furfuryl alcohol and furfural can be found in Figure S8. Furfural conversion and selectivity can be calculated by the following equations:

$$\text{Conversion (\%)} = \frac{n_0 - n_{\text{furfural}}}{n_0} \times 100\% \quad (1)$$

$$\text{Selectivity (\%)} = \frac{n_{\text{furfuryl alcohol}}}{n_0 - n_{\text{furfural}}} \times 100\% \quad (2)$$

where  $n_0$  is the initial concentration of furfural, the  $n_{\text{furfural}}$  is the furfural concentration after reaction, and the  $n_{\text{furfuryl alcohol}}$  refer to the concentration of furfuryl alcohol production.

All the applied potentials measured against Ag/AgCl can be converted to the reversible hydrogen electrode (RHE) scale by the following equation:

$$E(\text{V vs. RHE}) = E(\text{V vs. Ag/AgCl}) + 0.196 \text{ V} + 0.059 \times \text{pH} \quad (3)$$

#### 4. Conclusions

Bio-electrocatalysis hydrogenation of furfural for furfuryl alcohol production was realized by integrating the electro-chemical NADH regeneration and enzymatic catalysis by ADH. In this process, the synthesized Rh-complex was successfully fixed on the amino-modified carbon paper, and the as-prepared Rh-complex fixed electrode ensures sustainable and stable NADH regeneration under mild conditions. After combing the enzymic catalysis with the NADH regeneration in bio-electrocatalysis system, a high furfuryl alcohol selectivity of 81.5% at  $-0.43 \text{ V vs. RHE}$  was achieved. The current research showed promising green alternatives for the valorization of furfural and other biomass-derived compounds.

**Supplementary Materials:** The following supporting information can be downloaded at: <https://www.mdpi.com/article/10.3390/catal13010101/s1>, Figure S1: Flowchart for the preparation of the Rh-complex fixed electrode; Figure S2: Elemental mappings of the Rh-complex fixed electrode. The purple dots represent N element; Figure S3: XPS spectrum of (a) Cl 2p; (b) O 1s; and (c) C 1s; Figure S4: XRD patterns of the Rh-complex; Figure S5: The current densities of the bio-electrocatalytic hydrogenation of furfural under different applied potentials; Figure S6: The H-cell used in the bio-electrocatalytic hydrogenation of furfural; Figure S7: UV-vis standard curve of NADH at 340 nm; Figure S8: HPLC standard curves of furfuryl alcohol and furfural.

**Author Contributions:** P.Z. and X.L. designed the experiments, made the main contribution to the experimental works, and managed the experimental and writing process as co-first authors; Q.Z., C.Z. (Chenxi Zhang) and H.Z. assisted in accomplishing a part of the experimental works and characterizations; C.R. and J.Z. provided the concept of this research; C.Z. (Changwei Zhang) and S.Z. participated in the guidance of this work; D.C. provided advice on the work as the corresponding author. All authors have read and agreed to the published version of the manuscript.

**Funding:** This work was funded by the National Natural Science Foundation of China (Grant No. 22078018), the Natural Science Foundation of Beijing (Grant No. 2222016), and Bingtuan Science and Technology Program (Grant No. 2022DB025).

**Data Availability Statement:** All data are available upon reasonable request from the authors.

**Conflicts of Interest:** The authors declare no conflict of interest.

#### References

1. Teng, X.N.; Si, Z.H.; Li, S.F.; Yang, Y.H.; Wang, Z.; Li, G.Z.; Zhao, J.; Cai, D.; Qin, P.Y. Tin-loaded sulfonated rape pollen for efficient catalytic production of furfural from corn stover. *Ind. Crops Prod.* **2020**, *151*, 112481. [CrossRef]
2. Zhang, J.; Cai, D.; Qin, Y.; Liu, D.; Zhao, X. High value-added monomer chemicals and functional bio-based materials derived from polymeric components of lignocellulose by organosolv fractionation. *Biofuels Bioprod. Biorefining* **2020**, *14*, 371–401. [CrossRef]

3. Zhu, Q.; Zhuang, Y.; Zhao, H.; Zhan, P.; Ren, C.; Su, C.; Ren, W.; Zhang, J.; Cai, D.; Qin, P. 2,5-Diformylfuran production by photocatalytic selective oxidation of 5-hydroxymethylfurfural in water using MoS<sub>2</sub>/CdIn<sub>2</sub>S<sub>4</sub> flower-like heterojunctions. *Chin. J. Chem. Eng.* **2022**, *in press*.
4. Millan, G.G.; Sixta, H. Towards the green synthesis of furfuryl alcohol in a one-pot system from xylose: A review. *Catalysts* **2020**, *10*, 1101. [[CrossRef](#)]
5. Rodriguez, A.; Rache, L.Y.; Brijaldo, M.H.; Romanelli, G.P.; Luque, R.; Martinez, J.J. Biocatalytic transformation of furfural into furfuryl alcohol using resting cells of *Bacillus cereus*. *Catal. Today* **2021**, *372*, 220–225. [[CrossRef](#)]
6. Cao, Y.; Noël, T. Efficient electrocatalytic reduction of furfural to furfuryl alcohol in a microchannel flow reactor. *Org. Process. Res. Dev.* **2019**, *23*, 403–408. [[CrossRef](#)]
7. Chen, X.F.; Zhang, L.G.; Zhang, B.; Guo, X.C.; Mu, X.D. Highly selective hydrogenation of furfural to furfuryl alcohol over Pt nanoparticles supported on g-C<sub>3</sub>N<sub>4</sub> nanosheets catalysts in water. *Sci. Rep.* **2016**, *6*, 28558. [[CrossRef](#)]
8. Yu, H.B.; Zhao, J.H.; Wu, C.Z.; Yan, B.; Zhao, S.L.; Yin, H.F.; Zhou, S.H. Highly efficient ir-coox hybrid nanostructures for the selective hydrogenation of furfural to furfuryl alcohol. *Langmuir* **2021**, *37*, 1894–1901. [[CrossRef](#)]
9. Audemar, M.; Ciotonea, C.; Vigier, K.D.; Royer, S.; Ungureanu, A.; Dragoi, B.; Dumitriu, E.; Jerome, F. Selective hydrogenation of furfural to furfuryl alcohol in the presence of a recyclable cobalt/SBA-15 catalyst. *ChemSusChem* **2015**, *8*, 1885–1891. [[CrossRef](#)]
10. Audemar, M.; Wang, Y.; Zhao, D.; Royer, S.; Jerome, F.; Len, C.; De Oliveira Vigier, K. Synthesis of furfuryl alcohol from furfural: A comparison between batch and continuous flow reactors. *Energies* **2020**, *13*, 1002. [[CrossRef](#)]
11. Zhao, H.; Zhu, Q.; Zhuang, Y.; Zhan, P.; Qi, Y.; Ren, W.; Si, Z.; Cai, D.; Yu, S.; Qin, P. Hierarchical ZnIn<sub>2</sub>S<sub>4</sub> microspheres as photocatalyst for boosting the selective biohydrogenation of furfural into furfuryl alcohol under visible light irradiation. *Green Chem. Eng.* **2022**, *3*, 385–394. [[CrossRef](#)]
12. Gong, X.-M.; Qin, Z.; Li, F.-L.; Zeng, B.-B.; Zheng, G.-W.; Xu, J.-H. Development of an engineered Ketoreductase with simultaneously improved thermostability and activity for making a bulky atorvastatin precursor. *ACS Catal.* **2019**, *9*, 147–153. [[CrossRef](#)]
13. Dellomonaco, C.; Clomburg, J.M.; Miller, E.N.; Gonzalez, R. Engineered reversal of the  $\beta$ -oxidation cycle for the synthesis of fuels and chemicals. *Nature* **2011**, *476*, 355–359. [[CrossRef](#)]
14. Kang, C.; Hayes, R.; Sanchez, E.J.; Webb, B.N.; Li, Q.; Hooper, T.; Nissen, M.S.; Xun, L. Furfural reduction mechanism of a zinc-dependent alcohol dehydrogenase from *Cupriavidus necator* JMP134. *Mol. Microbiol.* **2012**, *83*, 85–95. [[CrossRef](#)] [[PubMed](#)]
15. Zhang, Z.; Muschiol, J.; Huang, Y.; Sigurdardóttir, S.B.; von Solms, N.; Daugaard, A.E.; Wei, J.; Luo, J.; Xu, B.-H.; Zhang, S.; et al. Efficient ionic liquid-based platform for multi-enzymatic conversion of carbon dioxide to methanol. *Green Chem.* **2018**, *20*, 4339–4348. [[CrossRef](#)]
16. Qin, L.Z.; He, Y.C. Chemoenzymatic synthesis of furfuryl alcohol from biomass in tandem reaction system. *Appl. Biochem. Biotechnol.* **2020**, *190*, 1289–1303. [[CrossRef](#)] [[PubMed](#)]
17. Ashkan, Z.; Hemmati, R.; Homaei, A.; Dinari, A.; Jamlidoost, M.; Tashakor, A. Immobilization of enzymes on nanoinorganic support materials: An update. *Int. J. Biol. Macromol.* **2021**, *168*, 708–721. [[CrossRef](#)]
18. Pietricola, G.; Chamorro, L.; Castellino, M.; Maureira, D.; Tommasi, T.; Hernández, S.; Wilson, L.; Fino, D.; Ottone, C. Covalent immobilization of dehydrogenases on carbon felt for reusable anodes with effective electrochemical cofactor regeneration. *ChemistryOpen* **2022**, *11*, e202200102. [[CrossRef](#)]
19. Li, B.; Li, Y.; Bai, D.; Zhang, X.; Yang, H.; Wang, J.; Liu, G.; Yue, J.; Ling, Y.; Zhou, D.; et al. Whole-cell biotransformation systems for reduction of prochiral carbonyl compounds to chiral alcohol in *Escherichia coli*. *Sci. Rep.* **2014**, *4*, 6750. [[CrossRef](#)]
20. Salic, A.; Zelic, B. ADH-catalysed hexanol oxidation with fully integrated NADH regeneration performed in microreactors connected in series. *RSC Adv.* **2014**, *4*, 41714–41721. [[CrossRef](#)]
21. Saba, T.; Burnett, J.W.H.; Li, J.; Kechagiopoulos, P.N.; Wang, X. A facile analytical method for reliable selectivity examination in cofactor NADH regeneration. *Chem. Commun.* **2020**, *56*, 1231–1234. [[CrossRef](#)]
22. Wu, H.; Tian, C.; Song, X.; Liu, C.; Yang, D.; Jiang, Z. Methods for the regeneration of nicotinamide coenzymes. *Green Chem.* **2013**, *15*, 1773–1789. [[CrossRef](#)]
23. Wang, X.D.; Saba, T.; Yiu, H.H.P.; Howe, R.F.; Anderson, J.A.; Shi, J.F. Cofactor NAD(P)H regeneration inspired by heterogeneous pathways. *Chem* **2017**, *2*, 621–654. [[CrossRef](#)]
24. Cahn, J.K.B.; Werlang, C.A.; Baumschlager, A.; Brinkmann-Chen, S.; Mayo, S.L.; Arnold, F.H. A general tool for engineering the NAD/NADP cofactor preference of oxidoreductases. *ACS Synth. Biol.* **2017**, *6*, 326–333. [[CrossRef](#)] [[PubMed](#)]
25. Ali, I.; Khan, T.; Omanovic, S. Direct electrochemical regeneration of the cofactor NADH on bare Ti, Ni, Co and Cd electrodes: The influence of electrode potential and electrode material. *J. Mol. Catal. A Chem.* **2014**, *387*, 86–91. [[CrossRef](#)]
26. Kochius, S.; Park, J.B.; Ley, C.; Koenst, P.; Hollmann, F.; Schrader, J.; Holtmann, D. Electrochemical regeneration of oxidised nicotinamide cofactors in a scalable reactor. *J. Mol. Catal. B Enzym.* **2014**, *103*, 94–99. [[CrossRef](#)]
27. Zhang, Z.B.; Vasiliu, T.; Li, F.F.; Laaksonen, A.; Zhang, X.P.; Mocci, F.; Ji, X.Y. Novel artificial ionic cofactors for efficient electro-enzymatic conversion of CO<sub>2</sub> to formic acid. *J. CO<sub>2</sub> Util.* **2022**, *60*, 101978. [[CrossRef](#)]
28. Song, H.-K.; Lee, S.H.; Won, K.; Park, J.H.; Kim, J.K.; Lee, H.; Moon, S.-J.; Kim, D.K.; Park, C.B. Electrochemical regeneration of NADH enhanced by platinum nanoparticles. *Angew. Chem. Int. Ed.* **2008**, *47*, 1749–1752. [[CrossRef](#)]
29. Hollmann, F.; Witholt, B.; Schmid, A. Cp\*Rh(bpy)(H<sub>2</sub>O)<sup>(2+)</sup>: A versatile tool for efficient and non-enzymatic regeneration of nicotinamide and flavin coenzymes. *J. Mol. Catal. B-Enzym.* **2002**, *19*, 167–176. [[CrossRef](#)]

30. Vuorilehto, K.; Lutz, S.; Wandrey, C. Indirect electrochemical reduction of nicotinamide coenzymes. *Bioelectrochemistry* **2004**, *65*, 1–7. [[CrossRef](#)]
31. Lee, L.G.; Whitesides, G.M. Enzyme-catalyzed organic synthesis: A comparison of strategies for in situ regeneration of NAD from NADH. *J. Am. Chem. Soc.* **1985**, *107*, 6999–7008. [[CrossRef](#)]
32. Yu, S.S.; Zhang, S.D.; Li, K.N.; Yang, Q.; Wang, M.; Cai, D.; Tan, T.W.; Chen, B.Q. Furfuryl alcohol production with high selectivity by a novel visible-light driven biocatalysis process. *ACS Sustain. Chem. Eng.* **2020**, *8*, 15980–15988. [[CrossRef](#)]
33. Zhang, L.; Etienne, M.; Vilà, N.; Le, T.X.H.; Kohring, G.-W.; Walcarius, A. Electrocatalytic biosynthesis using a Bucky paper functionalized by [Cp\*Rh(bpy)Cl]<sup>+</sup> and a renewable enzymatic layer. *ChemCatChem* **2018**, *10*, 4067–4073. [[CrossRef](#)]
34. Zhang, C.; Zhang, H.; Pi, J.; Zhang, L.; Kuhn, A. Bulk electrocatalytic NADH cofactor regeneration with bipolar electrochemistry. *Angew. Chem. Int. Ed.* **2022**, *61*, e202111804. [[CrossRef](#)] [[PubMed](#)]
35. Li, W.; Zhang, C.; Zheng, Z.; Zhang, X.; Zhang, L.; Kuhn, A. Fine-tuning the electrocatalytic regeneration of NADH cofactor using [Rh(Cp\*)(bpy)Cl]<sup>+</sup>-functionalized metal–organic framework films. *ACS Appl. Mater. Interfaces* **2022**, *14*, 46673–46681. [[CrossRef](#)]
36. Lin, G.; Zhang, Y.Y.; Hua, Y.T.; Zhang, C.H.; Jia, C.C.; Ju, D.X.; Yu, C.M.; Li, P.; Liu, J. Bioinspired metalation of the metal-organic framework MIL-125-NH<sub>2</sub> for photocatalytic NADH regeneration and gas-liquid-solid three-phase enzymatic CO<sub>2</sub> reduction. *Angew. Chem. Int. Ed.* **2022**, *61*, e202206283. [[CrossRef](#)] [[PubMed](#)]
37. Zhang, Z.; Li, J.; Ji, M.; Liu, Y.; Wang, N.; Zhang, X.; Zhang, S.; Ji, X. Encapsulation of multiple enzymes in a metal–organic framework with enhanced electro-enzymatic reduction of CO<sub>2</sub> to methanol. *Green Chem.* **2021**, *23*, 2362–2371. [[CrossRef](#)]
38. Zhang, L.; Vilà, N.; Kohring, G.-W.; Walcarius, A.; Etienne, M. Covalent immobilization of (2,2'-bipyridyl) (pentamethylcyclopentadienyl)-Rhodium complex on a porous carbon electrode for efficient electrocatalytic NADH regeneration. *ACS Catal.* **2017**, *7*, 4386–4394. [[CrossRef](#)]
39. Kim, S.-H.; Chung, G.-Y.; Kim, S.-H.; Vinothkumar, G.; Yoon, S.-H.; Jung, K.-D. Electrochemical NADH regeneration and electroenzymatic CO<sub>2</sub> reduction on Cu nanorods/glassy carbon electrode prepared by cyclic deposition. *Electrochim. Acta* **2016**, *210*, 837–845. [[CrossRef](#)]
40. Chen, Y.; Li, P.; Noh, H.; Kung, C.-W.; Buru, C.T.; Wang, X.; Zhang, X.; Farha, O.K. Stabilization of formate dehydrogenase in a metal–organic framework for bioelectrocatalytic reduction of CO<sub>2</sub>. *Angew. Chem. Int. Ed.* **2019**, *58*, 7682–7686. [[CrossRef](#)]
41. Zhan, P.; Yang, S.; Chu, M.G.; Zhu, Q.; Zhuang, Y.; Ren, C.; Chen, Z.Y.; Lu, L.; Qin, P.Y. Amorphous copper-modified gold interface promotes selective CO<sub>2</sub> electroreduction to CO. *ChemCatChem* **2022**, *14*, e202200109. [[CrossRef](#)]
42. Chambers, M.B.; Wang, X.; Elgrishi, N.; Hendon, C.H.; Walsh, A.; Bonnefoy, J.; Canivet, J.; Quadrelli, E.A.; Farrusseng, D.; Mellot-Draznieks, C.; et al. Photocatalytic carbon dioxide reduction with Rhodium-based catalysts in solution and heterogenized within metal-organic frameworks. *ChemSusChem* **2015**, *8*, 603–608. [[CrossRef](#)] [[PubMed](#)]
43. Luo, J.; Meyer, A.S.; Mateiu, R.V.; Kalyani, D.; Pinelo, M. Functionalization of a membrane sublayer using reverse filtration of enzymes and dopamine coating. *ACS Appl. Mater. Interfaces* **2014**, *6*, 22894–22904. [[CrossRef](#)] [[PubMed](#)]

**Disclaimer/Publisher's Note:** The statements, opinions and data contained in all publications are solely those of the individual author(s) and contributor(s) and not of MDPI and/or the editor(s). MDPI and/or the editor(s) disclaim responsibility for any injury to people or property resulting from any ideas, methods, instructions or products referred to in the content.